PHOTOELASTIC INVESTIGATION OF SUBMARINE FRAME PENETRATIONS

by

JOHN A. LEARY, II
Lieutenant, United States Navy
B.S., United States Naval Academy

Submitted in Partial Fulfillment of the Requirements for the
Degree of Naval Engineer
and the
Degree of Master of Science in Naval Architecture
at the

MASSACHUSETTS INSTITUTE OF TECHNOLOGY

May 1965

PHOTOELASTIC INVESTIGATION OF SUBMARINE FRAME PENETRATIONS

by

JOHN A. LEARY, II
Lieutenant, United States Navy
B.S., United States Naval Academy
(1958)

Submitted in Partial Fulfillment of the Requirements for the
Degree of Naval Engineer
and the
Degree of Master of Science in Naval Architecture
at the

MASSACHUSETTS INSTITUTE OF TECHNOLOGY

May 1965

PHOTOELASTIC INVESTIGATION OF SUBMARINE FRAME PENETRATIONS by JOHN A. LEARY, II. Submitted to the Department of Naval Architecture and Marine Engineering on 21 May 1965 in partial fulfillment of the requirements for the Master of Science degree in Naval Architecture and Marine Engineering and the Professional degree, Naval Engineer.

ABSTRACT

The object of this investigation is to determine relative stress concentration factors (SCFs) for penetrations in submarine structural frames.

Phase I concerned itself with elliptical penetrations with ratios of a/b (major axis/minor axis) from 1 (a circle) to 1.84. These penetrations were made in the center of Columbia Resin (CR-39) photoelastic plates with "a" approximately equal to 1". The plate sizes were originally 6" x 6" x $\frac{1}{2}$" and were reduced in size along the edge parallel to the major axis "a" during experimentation to simulate edge effect on the penetrations.

A biaxial compression field was applied to the model's edge with ratios of K (stress parallel minor axis "b"/stress parallel major axis "a") greater than one. Using a circular polariscope the isochromatic patterns were observed and the SCFs computed.

It was found that a circular hole penetration at a specified location always has a lower SCF than an elliptical hole with its major axis "a" equal to the circle's diameter and with the major axis parallel to the radial stress direction. This is true for values of K greater than one. It was also found that this advantage of circular holes is greater as the distance to the edge is decreased.

Phase II was to establish the relationship between SCFs for circular penetrations with the variables being web depth, flanges, and relative location in the submarine frame.

The first model was a $\frac{1}{2}$" thick circular ring of CR-39 with the outside diameter 8" and the inside diameter 5". Five $\frac{1}{4}$" circular holes were drilled in the model starting at a radius of 3 3/4" and incrementing inward in steps of 1/8" with 60° spacing between holes to prevent mutual interference.

The model was subjected to a hydrostatic pressure loading through a hoop loading cell. The isochromatic patterns were observed and the SCFs computed. This experiment was repeated with the addition of a flange on the inside edge, again without a flange but with the inside diameter increased to 6" (third model), and finally with the addition of a flange.

It was found that for the ratio of outside radius to inside radius of 1.60 (first model) the best location for the placement of a circular penetration with a diameter equal to 16.6% of the web's depth is 72.5% of the web's depth measured outward from the inside edge of the web. When the ratio decreased to 1.33 (third model) the best location approached to within 4.0% of the centerline of the web. The addition of flanges had the effect of moving the location slightly towards the center of the model. It was also found that deviation from the established location of minimum SCF for penetrations in a submarine web with flange should be in an outward radial direction to minimize the SCF.

Thesis Supervisor: John Harvey Evans

Title: Professor of Naval Architecture

ACKNOWLEDGEMENT

I wish to express my appreciation to the Electric Boat Division of General Dynamics Corporation for technical assistance, and to Professor Jerome Catz for his assistance and advice on experimental techniques. Grateful acknowledgement is due Professor John Harvey Evans for his valuable contributions, guidance, and encouragement. My wife, Nancy, I also acknowledge for her patience in typing the manuscript and proof.

J. A. L. II

TABLE OF CONTENTS

		Page
	Abstract	i
	Acknowledgement	iii
	Table of Contents	iv
	Figures and Tables	v
I.	Introduction	1
II.	Procedure	4
III.	Results	7
IV.	Discussion of Results	11
V.	Conclusions	16
VI.	Recommendations	18
VII.	Appendix	
A.	Details of Procedure	20
B.	Summary of Data and Calculations	27
C.	Sample Calculations	29
D.	Supplementary Discussion	31
E.	Original Data	35
F.	Literature Citations	48

FIGURES AND TABLES

		Page
Figure I	Plot of 2d/b versus SCF, Phase I.	9
Figure II	Plot of radial distance to hole versus SCF, Phase II.	10
Figure III	Loading device for biaxial compression, Phase I.	25
Figure IV	Loading device for hydrostatic pressure, Phase II.	26
Figure V	Calibration of photoelastic material through tension test, Phase I.	35
Figure VI	"K" versus SCF for 6" x 6" models, Phase I.	36
Figure VII	"K" versus SCF for 6" x 5" models, Phase I.	37
Figure VIII	"K" versus SCF for 6" x $4\frac{1}{2}$" models, Phase I.	38
Figure IX	"K" versus SCF for 6" x 4" models, Phase I.	39
Figure X	"K" versus SCF for circle model, Phase I.	40
Figure XI	"K" versus SCF for ellipse, a/b = 1.11, Phase I.	41
Figure XII	"K" versus SCF for ellipse, a/b = 1.42, Phase I.	42
Figure XIII	"K" versus SCF for ellipse, a/b = 1.84, Phase I.	43
Figure XIV	Nomograph to directly relate fringe order at any radius "r" to hydrostatic pressure, Phase II.	44
Figure XV	Sample of stress patterns and stress gradients, Phase II.	45
Table I	Summary of Data and calculations, Phase I.	27
Table II	Summary of data and calculations, Phase II.	28
Table III	Fringe orders versus radius, Phase II.	46

I. INTRODUCTION

Penetrations in submarine frames are an ever increasing problem that submarine design engineers have to face. The deeper the submarines of today and the future go, the more evident the problem will become. The present state of the art of penetrations is limited to a few common cases, and an overall attack on the subject is lagging behind the needs of the design engineer of today.

A publication issued by the Navy Bureau of Aeronautics states, "While minor improvement in fatigue life may be accomplished merely by changing material, few serious fatigue difficulties have been corrected in this way. Such difficulties are almost always traceable to improper design, fabrication, and maintenance. . . By studying stress concentration factors much can be learned about how to produce designs that are superior from the standpoint of resistance to repeated loads and how to evaluate approximately the influence of various geometric features."

Every penetration in a structural member carrying loads causes the formation of stress concentrations. If these penetrations are close to the edge, large relative to the width of member, or in close proximity to each other, the stress concentrations are increased. If the stress concentrations are prohibitive, steps must be taken to alleviate the problem.

The data to date applies only to several classes of penetrations and loading conditions. This limited supply of information causes a design engineer, when faced with an unknown penetration situation, to

either restrict the load to a smaller portion than actually possible or to overdesign the structural member. Since computations of unknown penetrations are tedious and long, and methods often nonexistent, overdesign is the avenue of approach to be on the safe side. This overdesign cannot be accepted in the high strength metals used in submarines of today and the future, since the deep diving submarine is becoming a weight critical structure as the depths are increased.

The methods of analysis to determine stress concentrations may be through mathematical calculations, full scale studies, and model studies. The mathematical calculations for penetrations are mainly limited to symmetrical models with large exterior dimensions relative to the dimension of the penetration. The restrictions of this method make it unfeasible for submarine frame analysis. Full scale studies are impractical due to the enormous size of submarine frames and the expense that would be involved. Model analysis using photoelasticity has therefore been chosen as the best method to aid the designer of submarine frame penetrations.

Applying the photoelastic method to models of submarine penetrations is inexpensive, rapid, and accurate. This is the best method to analyze the deficiency in a given shaped penetration, to determine how to correct it, and to check the final solution. The intention of this paper is to accomplish this analysis.

Phase I of this experiment was to establish the relative stress concentration factors between ellipses of various a/b (major axis/minor axis) ratios and various edge distances. This was performed in a stress

field similar to that existing in a submarine structural frame under hydrostatic pressure loading.

Phase II of this experiment was to establish the relationship between stress concentration factors for circular holes in submarine frames with the variables being web depth, flanges, and relative location in the frame.

II. PROCEDURE

PHASE I.

The photoelastic material chosen for this experiment was Columbia Resin hereafter referred to as CR-39. This material is a clear material with good photoelastic properties in compression loading and good machining characteristics. See Appendix A. In a meeting with Mr. E. Chapman of Chapman Laboratories, the fact was stressed that by using CR-39 one gets the maximum experimental return on money used for photoelastic material. This was a contributing factor in choosing CR-39 since minimum cost was one objective of this experiment.

Four models were made with nominal dimensions 6" x 6" x $\frac{1}{2}$" with different type holes machined in their respective centers. The holes, or penetrations, investigated were a circle and ellipses with a/b equal to 1.11, 1.42, and 1.84. The approximate length of the major axes in the above cases was 1".

A tensile specimen was machined in conjunction with the machining of the models as described in Appendix A. This tensile specimen was used to determine the photoelastic fringe constant of the material. See Appendix E, Figure V.

The models were placed in a biaxial compression loading frame described in Appendix A. The load parallel to the major axis was varied in increments from 0% to 100% of the load parallel to the minor

axis.

As the side load was varied in increments, the isochromatic pattern created by using a polariscope with circular polarized light with a dark field was observed, recorded, and photographed. The main purpose of this phase was to determine stress concentration factors, so data was only recorded at the intersections of the major and minor axes with the edge of the penetration. This data was then converted to stress concentration factors as shown in Appendix C.

After the above testing of models and recording and conversion of data, a portion of the model parallel to the major axis of the penetration was removed on one side to simulate edge effect. The same experimental procedure was then repeated.

PHASE II.

CR-39 was used for this phase for the same reasons as stated in Phase I.

A circular ring model was made from CR-39 to represent a submarine structural frame. The outside diameter was 8" and the inside diameter was 5". The model was $\frac{1}{2}$" thick. Five $\frac{1}{4}$" circular holes were drilled in the model starting at a radius of 3 and 3/4 " and incremented inward in steps of 1/8". These holes were spaced at equal angles of 60°(reference the geometric center of the model). The 60° provided more than adequate distance between holes to prevent mutual interference between hole fringe patterns when loaded.

The model was then placed in a hoop loading cell described in

Appendix A. As described in Appendix A, the loading cell read simulated pressure directly. The model was then subjected to a given pressure.

At a given pressure the isochromatic patterns created by using a polariscope and alternating dark and light field were drawn on tracing paper. This was done for each of the five circular penetrations.

The objective was to find the location in the stress field containing the minimum stress concentration factor for a circular hole.

After the above testing a $1\frac{1}{2}$" wide $\frac{1}{4}$" thick Cadco cast acrylic resin tube was attached to the inner surface of the model to simulate flange effect. This flange was attached with epoxy cement since CR-39 is insoluble and cannot be joined by conventional methods. The model was then subjected to the same pressure as before and the isochromatics again recorded.

The model was then machined to remove the flange and make the inside diameter of the model 6". The experiment was conducted with this geometric configuration. A flange of the same cross sectional dimensions as previously stated was then attached and the experiment repeated.

III. RESULTS

PHASE I.

The best evaluation of the results is by relative comparison of the stress concentration factors for the penetrations under variation of edge distance. A range of K (the ratio of $\sigma_{nominal}$ parallel minor axis/$\sigma_{nominal}$ parallel major axis) values from about 1.0 to ∞ were used to determine the stress concentration factors at the intersection of the major and minor axes with the elliptical holes. Only the value K equal to 5.0 will be presented in these results. K equal to 5.0 was chosen because it represents the approximate ratio of the actual stresses in present day submarine structural frames under hydrostatic pressure. The values of the stress concentration factors computed for the intersection of the minor axes with the elliptical holes are not included in this paper since they were not the governing factor.

K=5.0

	6"x6" MODEL		6"x5" MODEL		6"x4½" MODEL		6"x4" MODEL	
SHAPE a/b	2d/b*	SCF	2d/b	SCF	2d/b	SCF	2d/b	SCF
Circle 1.00	6.05	2.39	3.94	2.49	2.94	2.58	1.94	2.70
Ellipse 1.11	5.85	2.47	3.78	2.59	2.82	2.67	1.87	2.91
Ellipse 1.42	7.45	2.58	5.02	2.64	3.79	2.72	2.66	3.10
Ellipse 1.84	9.74	2.68	6.40	2.71	4.27	2.86	3.16	3.26

*2d/b = ratio of ½ minor axis dimension/edge distance measured from center of hole to near edge.

These results are plotted in Figure I.

Photographs were taken in conjunction with values of K equal to about 5.0. These photographs showed the trend visually indicated by the above table and Figure I.

PHASE II.

For this phase the stress concentration factor is defined as the ratio of the largest stress observed at the edge of a penetration to the theoretical maximum stress existing in the ring frame without penetrations but with the same hydrostatic loading.

The stress concentration factors were computed for both sides of the penetrations in a radial direction. The maximum stress without penetrations for each model investigated was the circumferential stress at the inner surface of the model. The stress gradients are represented in Appendix E, Figure XV.

For presentation and comparison purposes see Figure II. This Figure presents the maximum stress concentration factor as defined above for each hole with the independent variable being the radial distance to the center of that hole. The four model configurations are plotted together for relative comparison. This comparison is independent of the magnitude of the hydrostatic loading, since the stress concentration factors are constant with the linear variation of stresses that exist for this loading system.

FIGURE I.

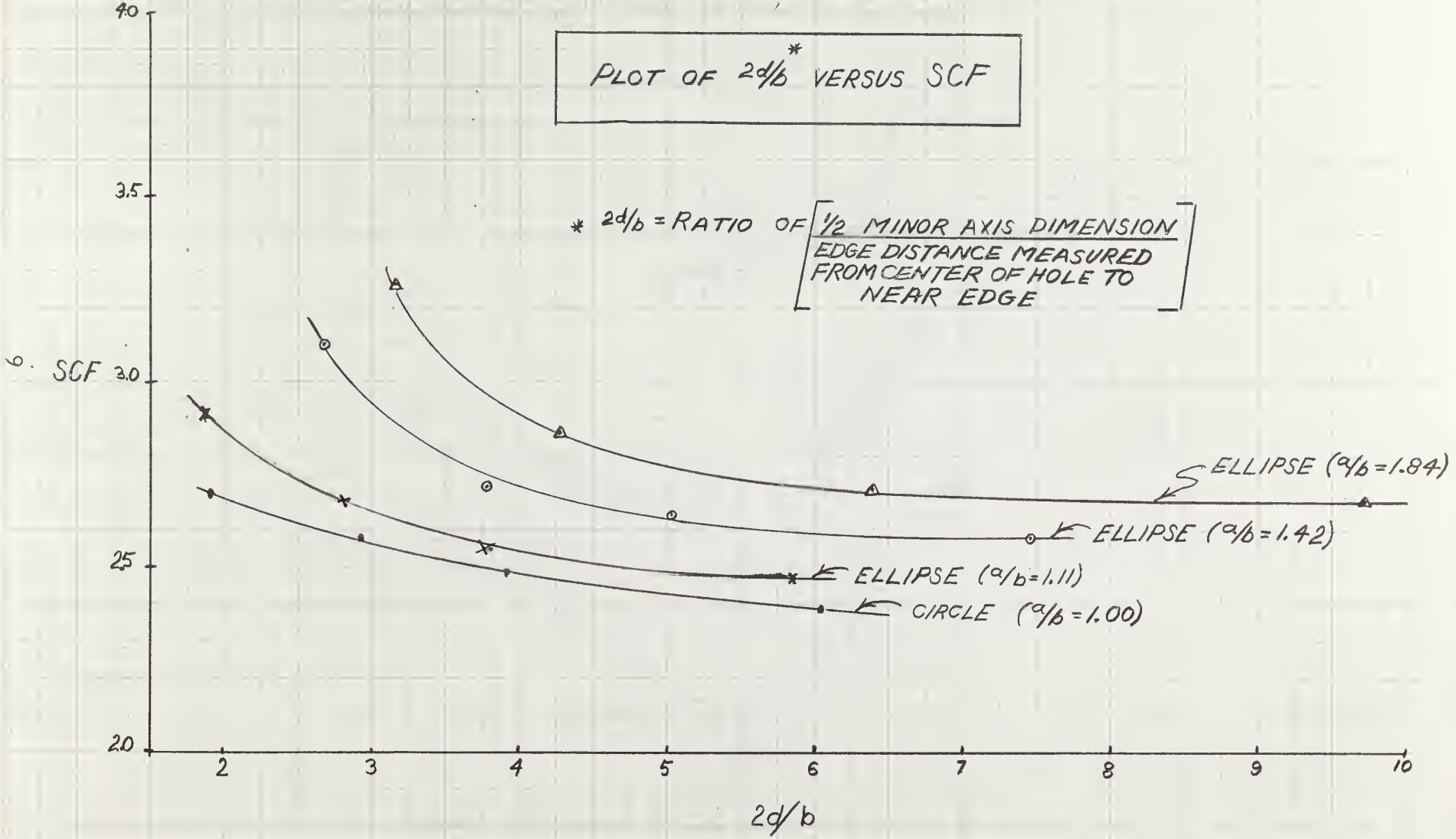

JAS 4/65

FIGURE II.

PLOT OF RADIAL DISTANCE TO HOLE VERSUS STRESS CONCENTRATION FACTOR

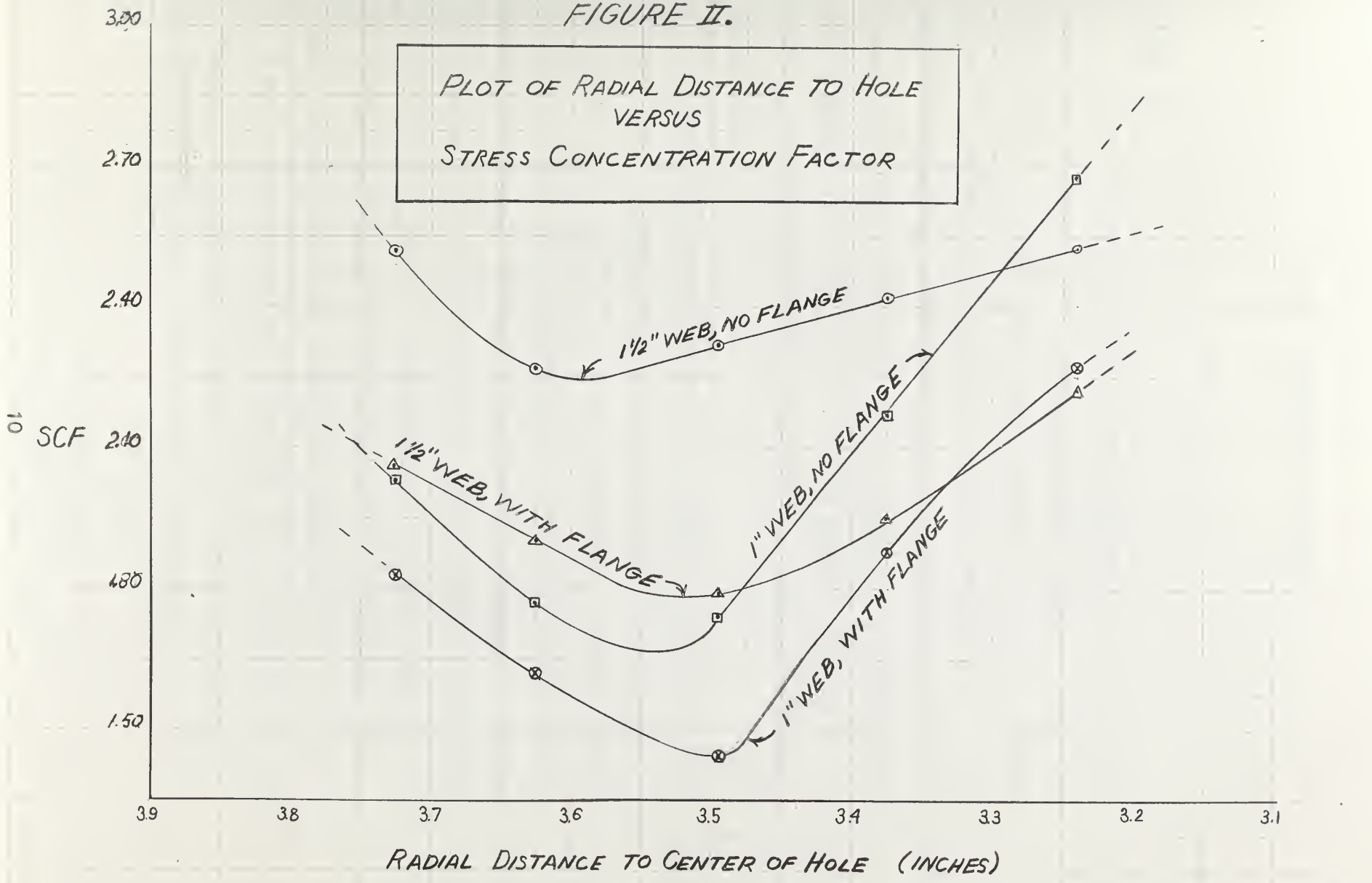

JAL 4/65

IV. DISCUSSION OF RESULTS

PHASE I.

The geometry of the problem under consideration in this thesis makes absolute quantitative correlation quite difficult. The model plate size of six inches square with approximately one inch holes was chosen to represent an infinite field prior to machining off of the edge to produce edge effect. This ratio of plate width to hole diameter (6:1) was chosen based on work by Durelli and Murray (4)* and by Griffel (8). The ratio of the hole diameter to plate thickness (2:1) is also a geometric factor governing the absolute quantitative correlation.

The method of loading described in Appendix A tends to have a lesser degree of experimental error as the value of K increases. This is evident on the plot of the circle and ellipse (a/b=1.84) of the 6"x6" models(Appendix E, FigureVI). The reason for this tendency is that it is extremely difficult to get perfect allignment of loading blocks on all four sides of the model. As the side load decreases (K increases) any degree of misallignment is lessened since the predominance of loading in only one direction is increased. This is a more accurate and precise loading configuration.

This loading problem was evident early in experimentation. As a double check on the data recorded and the visual symmetry of the

*Numbers in parentheses refer to Literature Citations.

biaxial compression field, a series of uniaxial compression runs were made. First a run was made with a single load applied parallel to the major axis and then with a single load applied parallel to the minor axis. Using the theory of superposition this data was combined to produce the desired biaxial compression field. If there were errors evident, further testing was performed to bring about correlation between the two methods.

Two properties of the model material, CR-39, caused some difficulty in obtaining accurate results. The first and major was the formation of residual stresses along the boundaries of the holes with time. This was retarded to some degree by the use of an air conditioning unit and a desiccator. This undesirable property is inherent with materials suitable for photoelasticity. The best solution to this problem, that of machining a small amount of material off the edge immediately prior to using the model, was not possible since the testing of sixteen configurations spanned a period of fifteen days. The other problem, though minor, was the slight effect of optical creep upon loading. This was minimized by not keeping the loads on over long periods of time and also through the uniaxial loading method mentioned previously. When running the uniaxial load test, readings were taken with increasing increments to maximum load and then the reverse was performed. Any difference between the two loading directions showed up as a kind of optical hysteresis loop.

Although CR-39 is brittle and has a tendency to chip while machining, little difficulty was experienced as long as the machining

was done slowly and carefully with the high speed Chapman cutter. Some slight edge stresses were induced with the Chapman cutter due to the heat effect produced by the cutting tools. For this reason, the readings of fringes were taken at points located very slightly in from the edge of the hole. These points were scribed on the models to insure the taking of readings at exactly the same reference point. This is probably a contributing factor to the absolute value of the stress concentration factor for the 6" x 6" model with a centered circular hole being low when compared to theory.

From Figure I it is indicated that the circular hole has a lower stress concentration than the elliptical hole when compared on the basis of equal ratios of 2d/b ($\frac{1}{2}$minor axis dimension/edge distance measured from center of hole to near edge). It is also evident that the stress concentration factor increases at a greater rate for increasing a/b ratios as the value of 2d/b decreases (Appendix E, Figures VI through XIII).

When the results are compared on the basis of equal amounts of edge removed from each model (Appendix E, Figures VI through IX), there is approximately a constant increase in SCF (stress concentration factor) between models regardless of the value of K.

Murray (4) states what the trend of the relationship between a circle and an ellipse with a/b equal 2.0 in an infinite stress field (6" x 6" model with 1" hole) with similar value of K should be relative to SCF's. This trend was established as being correct (Appendix E, Figure VI).

PHASE II.

The smallest ratio (outside radius/inside radius) that was experimented with was 1.33. The value of this ratio that exists for present day submarine frames is about 1.15. The 1.33 was chosen as a "feasibility" step to smaller ratios.

The stress gradients were recorded in the form of fringe diagrams so as to extrapolate to the very edges of the holes. By this method the extrapolated fringe values represent only circumferential stresses instead of the algebraic sum of principal stresses. This is because the radial stresses go to zero at the free boundaries of the holes being analyzed.

The major problem experienced in loading the model was that of indicated strain readings drifting when applying load through the stainless steel hoop. This was mainly attributed to the load cell's sensitivity to bending.

Due to this problem, more weight should be given to the results as represented by Figure II on an absolute basis than on the relative basis of SCF differences between individual curves. Lesser problems were those due to optical creep and residual stresses of the material similar to those discussed in Phase I. The residual stress problem was minimized since the total time lapse for the testing of the four models was only five days.

Minor bending might have been introduced into the results due to slight variations in concentricity. This was avoided to the best degree possible with the equipment available for the machining of the

models.

From Figure II it is indicated that a $\frac{1}{4}$" hole at a radius of 3.59" in a unreinforced web frame of 4" outside radius and a $2\frac{1}{2}$" inside radius has a minimum SCF as defined in the results. This minimum SCF is reduced by 21% through the addition of a $\frac{1}{4}$" by $1\frac{1}{2}$" flange with the same hydrostatic loading. The location for this minimum SCF is shifted towards the geometric center of the web by 0.07" to a radius of hole center equal to 3.52".

For the 4" outside radius and 3" inside radius unreinforced web, the minimum SCF for a $\frac{1}{4}$" hole is located at a radius of 3.54". With the addition of a flange of the same size as described above, this minimum SCF is reduced by 14% and shifted 0.04" inward to a radius equal to 3.50".

From the slopes of the curves, it is indicated that for the $1\frac{1}{2}$" unreinforced web frame it is advantageous to deviate in the inward direction from the point of minimum SCF to minimize the SCF. With the addition of the flange it makes little difference which direction is chosen from the minimum SCF to minimize the SCF.

For the 1" unreinforced and reinforced web frame it is quite evident that if need arises to deviate from location of minimum SCF it should definitely be done in an outward radial direction.

The effect of the closeness of the flange to the hole at radius 3.24" in the 1" wide web is evident as the curve of SCF's has a reverse curvature at that radius.

V. CONCLUSION

PHASE I.

A circular hole penetration in a submarine structural frame at a specified location always has a lower stress concentration factor than an elliptical hole with its major axis equal to the circle's diameter and with the major axis parallel to the radial stress direction. This is true for values of K greater than one.

As the ratio of 2d/b for a penetration of a given a/b ratio is decreased the stress concentration factor increases at a rate greater than 2d/b. This rate also increases as the ratio a/b increases. This means that the advantages of circular holes versus elliptical holes orientated as in above paragraph in submarine penetrations are more pronounced as the edge or boundary distance is decreased.

PHASE II.

For a hypothetical ratio of outside radius to inside radius of 1.60 for a submarine frame, the best location for the placement of a penetration is not in the center of the web depth. For a circular hole with a diameter equal to 16.6% of the web's depth the best location is 72.5% of the web's depth measured outward from the inside edge of the web. This 72.5% is reduced slightly with the insertion of a flange on the inside edge of the web.

For a ratio as defined above equal to 1.33, which more closely approaches the actual submarine ratio of 1.15, the best location for

for the placement of a circular penetration is close to the center of the web's depth. For a circular hole with a diameter of 25.0% of the web's depth, the best location is only 4.0% off the centerline of the web in the outward direction. Again, there is the same effect on this location with addition of a flange as in the above paragraph.

Deviations from the established locations of minimum SCF for penetration in a submarine web with flange become critical as illustrated below.

CASE	RADIUS	SCF
I	3.625 units	1.62
Minimum	3.495 units	1.44
II	3.365 units	1.92

for: outside radius of web = 4.0 units
inside radius of web = 3.0 units
hole diameter = 25% of web depth

In Case I the deviation from the radius of minimum SCF was 13% of web depth radially outward and its corresponding increase on minimum SCF was 12.5%. In case II the deviation from the radius of minimum SCF was the same amount but radially inward and the corresponding increase on minimum SCF was 33.4%.

The deviation in the above example is probably even more pronounced as the actual submarine radii ratio of 1.15 is approached.

VI. RECOMMENDATIONS

GENERAL

Every effort should be made to keep the time lag between the final cut in a photoelastic model close to where fringe readings will be taken and the actual recording of data as short as possible. In conjunction with this, a photoelastic laboratory with closely controlled temperature and low humidity would be of great aid in preventing time edge effect.

Use fast "accurate" loading to prevent optical creep which may cause experimental error at high stress levels. By the word "accurate" is meant direct reading load cells. Direct reading load cells indicate loads at the point of application and not at a remote location as using a remote pressure gage to indicate pressure in a hose that is supposedly transmitting that pressure through a hose to a model. (1)

PHASE I.

It is strongly recommended that all experimental work with biaxial stresses use the principle of superposition as a cross check on data. This applies to values of K from $-\infty$ to $+\infty$.

One study that would prove useful is varying the a/b ratio of the ellipse in an approximate infinite field with values of K from -1 to +1. Murray (4) has shown that for K between -0.50 to +0.65 an ellipse with a/b equal to 2 gives a lower stress concentration than a circle. By varying a/b from 1 to a value of about 3 in increments, a

plot of minimum stress concentrations less than that of a circle could be established. By varying edge distance parallel to the major axis with the same range of K another variable could be incorporated into the stress concentration factor of ellipses. The results of an investigation of the type mentioned above for values of K of about +0.20 would be applicable to submarine frames.

PHASE II.

The results of this phase prove the feasibility and also indicate the value to be gained by further work along the same lines. The radii ratio could now be reduced to 1.15 and experimentation done with the same variables -- circular hole location and flange effect and possibly with other variables as hole interaction between closely spaced holes, ellipses, and reinforcement of penetrations.

A model with a ratio of 1.15 would have larger dimensions than the ones worked with in this phase. The problem of concentricity will be more evident in the form of bending stresses which means that the accuracy of machining would become more critical.

It is recommended that a study be made into the reduction or elimination of the sensitivity of the load cell to bending if such a load cell were to be used for further experimental work along these lines.

VII. APPENDIX

A. DETAILS OF PROCEDURE

PHASE I.

Prior to the construction of the models, brass elliptical templates were manufactured. This was done by using a panograph machine which followed elliptical plastic templates and reproduced their shapes in brass at a 2:1 reduction in dimension.

The models were rough cut to within about 1/8" of the chosen shape using a jigsaw. Straight edge brass templates and the above elliptical brass templates were then attached to the rough model. These templates served as guides to the finished model shape.

The finished model shape was obtained using a Chapman high speed tungsten carbide rotary cutter. This high speed and the sharp tungsten carbide teeth prevents the introduction of heat stresses in the edges of the model. Therefore, annealing to remove stresses after machining is eliminated. Also edge polishing is not necessary since the cutter leaves an extremely smooth surface.

The tensile specimen shown in Appendix E, Figure V was made the same way as above using a brass template as a guide in the machining process.

The loading frame is shown in Figure III. The four loading surfaces in contact with the model were made from rolled steel. These were polished to a true flat mirror surface on plate glass with fine emery cloth. They were then scribed and labeled to facilitate accurate positioning of the model in the loading frame. Mineral oil was used

between model and loading surfaces to ensure uniform contact pressure.

Two load cells were used for this experiment. The top load cell was a dial indicator which read deflections of a calibrated load spring to the degree of accuracy of a few pounds. The load was transmitted to the top load cell by a double acting hydralic cylinder supplied with pressure by means of hand pumps. The side load cell was a "double beam type". It consisted of eight strain gages and had double the output of a single strain gage plus a high degree of sensitivity. It was hooked into a strain indicator which was calibrated to read resistance changes to the degree of accuracy of a few pounds. The load was transmitted to the side load cell by a single acting hydraulic cylinder supplied with pressure by means of another hand pump.

For the first size of the models (6" x6"), the top load was held at 600 pounds and the side load varied in increments of 100 pounds from 0 to 600 and back down from 600 to 0. This reversal in side load was done to check for optical creep of the material. The 600 pounds was chosen to give adequate values of fringe orders and at the same time not encounter a buckling problem in the model. To cross check data by the principle of superposition, some runs were made with zero side load, top load varying from 0 to 600 and back down from 600 to 0, in increments of 100 pounds. The same process was used for the side load with the top load equal to zero.

After the above testing the sizes were reduced as shown in Figure III and a similar procedure for loading as above was followed.

PHASE II.

Before starting this phase an extensive study was made to find the best method of simulating hydrostatic pressure for a ring frame from the point of view of accuracy of the data and cost.

One avenue persued was that of the hydraulic loading system similar to the one used by Cober.(2) This method was eliminated due to the approximate cost being several hundred dollars and the question of feasibility.

The method decided upon was quite simple in principal, low in cost, and proved effective. This method used a stainless steel band to apply a uniform hoop stress. An Aero-Seal worm drive clamp, primarily used for hoses, was tested on a sample model 6" in diameter. The Aero-Seal clamp was tightened by means of a screw driver. This feasibility test run proved the effectiveness of the method, but not enough torque could be applied to the clamp through the screw driver.

A "Band-It Tool" was then discovered to exist. This tool could apply a force of 1875 pounds in a stainless steel band of 5/8" width and in any diameter. This 1875 pounds was more than enough hoop stress to simulate hydrostatic loading.

The following method was then developed to directly measure the hydrostatic pressure caused by the stress in the stainless steel band.

From Timoshenko's (18) thick wall cylinder theory (external pressure only) the radial and tangential stresses at various radii were computed. From these stresses the differences $(\sigma_t - \sigma_r)$ were related to pressure directly through the argument of radius in Appendix E, Figure XIV. The

differences ($\sigma_t - \sigma_r$) were used since isochromatic fringe order readings represent these differences directly.

After calibration of a tensile specimen as done in Phase I, the fringe order was added to the nomograph. Now, at any given load in the band around the model, the fringe order at a particular radial distance could be observed and directly related to pressure.

The measurement of the load in the band was accomplished by using two SR-4 Type A-3 strain gages and a Strainsert Strain Indicator.

The advantage of this system was that once calibrated for the model without holes, the strain readings represent the same hydrostatic pressure regardless of changes in inside diameter, flanges, or penetrations.

Various combinations of rubber, teflon paper, and mineral oil were experimented with between the stainless steel band and the model to reduce stress concentrations due to machining. The best combination was a thin rubber band directly under the steel band and a piece of teflon paper between the rubber and the model as shown in Figure IV.

The stress concentration mentioned above arose from machining. The Chapman high speed cutter was not used for this phase but rather a machine lathe at a low RPM.

One problem that had to be overcome or reduced was the fabrication of stress and chip free $\frac{1}{4}$" holes. The size of the high speed tungsten carbide cutters precluded their use for these holes. All combinations of drill RPM and drilling rate were tested. The faster the drill RPM, the more residual stresses but the less chipping around

the surfaces of the hole. The slower the drill RPM, the less residual stresses but more chipping. The best combination was found to be that using a low RPM. The start of the hole was done at a slow drilling rate followed by a fast drilling rate and again a slow drilling rate as the drill broke through the other side of the model.

FIGURE III.

LOADING DEVICE FOR BIAXIAL COMPRESSION

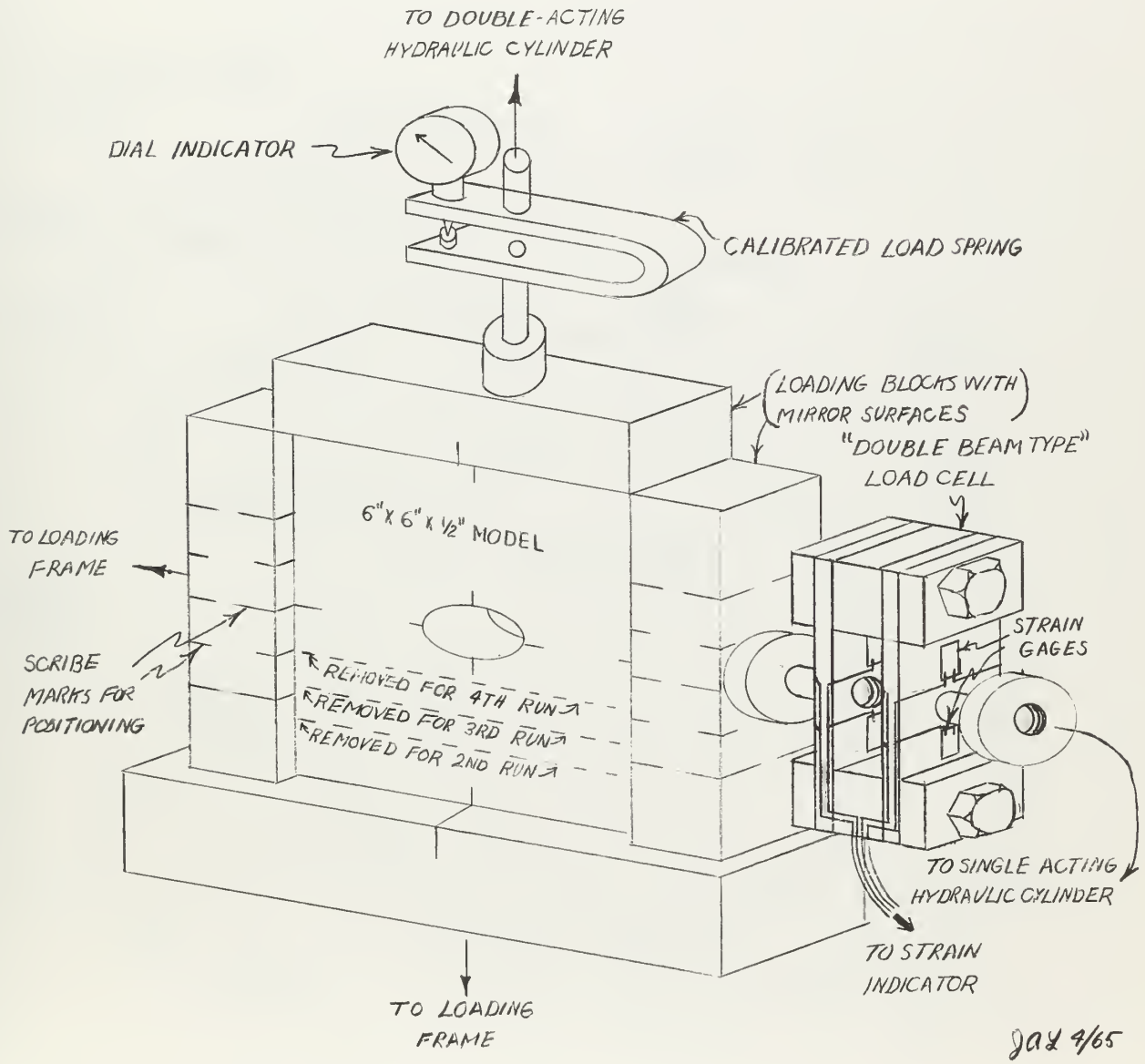

FIGURE IV.

LOADING DEVICE FOR HYDROSTATIC PRESSURE

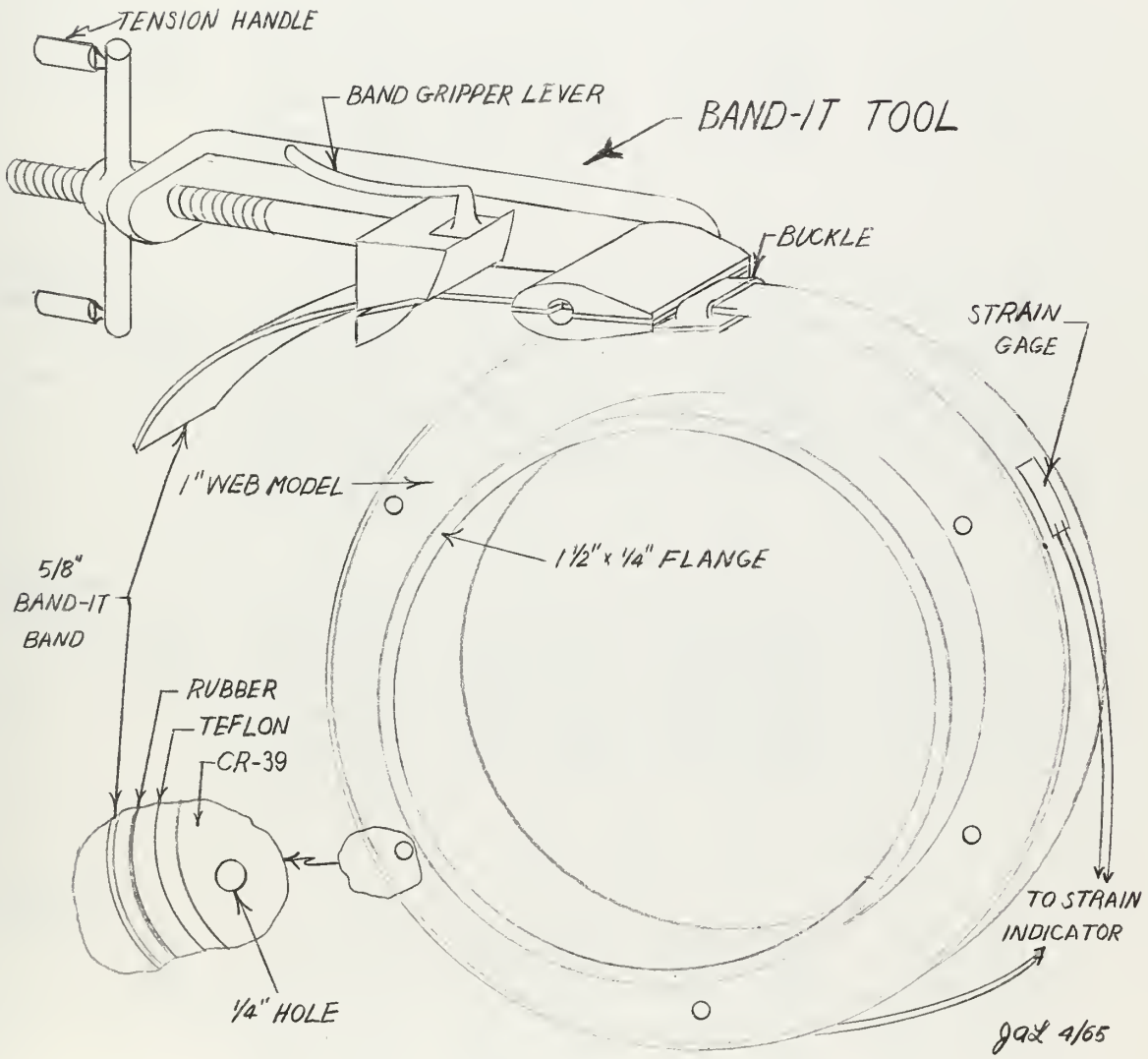

B. SUMMARY OF DATA AND CALCULATIONS

TABLE I.

PHASE I.

PENETRATION SHAPE	6"x6"MODEL		6"x5"MODEL		6"x4½"MODEL		6"x4"MODEL	
	K	SCF	K	SCF	K	SCF	K	SCF
Circle	1.00	1.64	0.95	1.80	0.93	1.93	0.89	2.13
(a/b = 1.00)	1.20	1.78	1.19	1.95	1.16	2.12	1.11	2.26
a = 1.00"	1.50	1.92	1.58	2.10	1.54	2.24	1.48	2.34
σ_{n1} = 245PSI	2.01	2.10	2.38	2.28	2.31	2.36	2.22	2.53
	2.99	2.26	4.80	2.49	4.62	2.57	4.46	2.69
	5.98	2.42	∞	2.71	∞	2.73	∞	2.82
	∞	2.62						
Ellipse								
(a/b = 1.11)	1.03	1.60	0.98	1.83	0.94	2.10	0.90	2.31
a = 1.16"	1.24	1.75	1.22	1.97	1.18	2.21	1.13	2.44
σ_{n1} = 253PSI	1.55	1.89	1.62	2.11	1.57	2.32	1.51	2.60
	2.07	2.12	2.44	2.34	2.36	2.48	2.26	2.72
	3.09	2.32	4.87	2.54	4.68	2.66	4.52	2.90
	6.18	2.53	∞	2.75	∞	2.78	∞	3.06
	∞	2.67						
Ellipse								
(a/b = 1.42)	1.07	1.86	1.03	2.02	1.01	2.21	0.98	2.70
a = 1.15"	1.28	1.96	1.28	2.14	1.26	2.30	1.22	2.79
σ_{n1} = 253PSI	1.60	2.10	1.71	2.26	1.69	2.40	1.63	2.90
	2.14	2.28	2.58	2.42	2.53	2.57	2.43	2.98
	3.20	2.44	5.18	2.65	5.06	2.72	4.86	3.10
	6.50	2.64	∞	2.89	∞	3.00	∞	3.20
	∞	2.86						
Ellipse								
(a/b = 1.84)	1.13	2.00	1.10	2.16	1.08	2.50	1.06	2.90
a = 1.14"	1.36	2.11	1.37	2.32	1.36	2.53	1.32	2.98
σ_{n1} = 2 58PSI	1.70	2.16	1.83	2.36	1.80	2.64	1.77	3.06
	2.26	2.40	2.64	2.48	2.58	2.71	2.66	3.18
	2.98	2.52	5.50	2.73	5.38	2.89	5.27	3.26
	5.95	2.74	∞	3.03	∞	3.16	∞	3.39
	∞	3.00						

TABLE II.

PHASE II.

RADIUS TO HOLE'S CENTER	SCF FOR 1½" WEB WITHOUT FLANGE	SCF FOR 1½" WEB WITH FLANGE	SCF FOR 1" WEB WITHOUT FLANGE	SCF FOR 1" WEB WITH FLANGE
3.725"	2.52	2.06	2.03	1.83
3.625"	2.27	1.90	1.77	1.62
3.495"	2.32	1.79	1.74	1.44
3.375"	2.42	1.95	2.17	1.88
3.245"	2.62	2.22	2.68	2.27

C. SAMPLE CALCULATIONS

PHASE I.

Calculations for the ellipse (a/b = 1.84) with 2" cut off edge parallel to "a" axis with 80 pound side load.

DIMENSIONS

L = 5.95"

W = 4.00"

t = 0.488"

a = 1.14"

b = 0.62"

READINGS

P_1 = 600 lbs.

P_2 = 80 lbs.

n = 4.27 orders

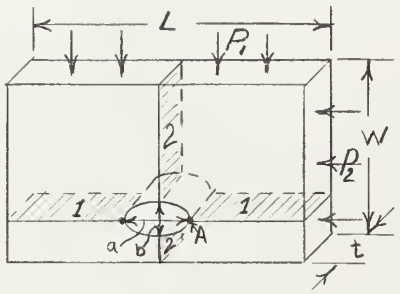

Net sectional area of 1 = (L-a)t = (5.95-1.14)0.488 = 2.34 in^2 = A_1

Net sectional area of 2 = (W-b)t = (4.00-0.62)0.488 = 1.64 in^2 = A_2

The nominal stress based on net section area after removal of elliptical hole = $P/A = \sigma_n$

$$\sigma_{n1} = P_1/A_1 = 600/2.34 = 258 \text{ PSI}, \quad \sigma_{n2} = P_2/A_2 = 80/1.64 = 49 \text{ PSI}$$

$$K \equiv \text{the ratio } \sigma_{n1}/\sigma_{n2} = 258/49 = 5.27$$

The fringe constant of this material as determined in Appendix E, Figure V was 96lbs/(in)(order).

$$\sigma_1 - \sigma_2 = fn/t \text{ (Shown in Supplementary Discussion)}$$

Since we are at the free boundary when taking readings of fringe orders at "A", $\sigma_2 = 0$, and

$$\sigma_1 = (96)(4.27)/0.488 = 840 \text{ PSI} = \sigma_{max\ A}$$

Stress concentration factor $\equiv \sigma_{max}/\sigma_n$ = SCF

$$SCF_A = 840/258 = 3.26$$

PHASE II.

Calculations for the 1" web model without flange for hole at radius 3.495" with a hydrostatic load of 100 PSI.

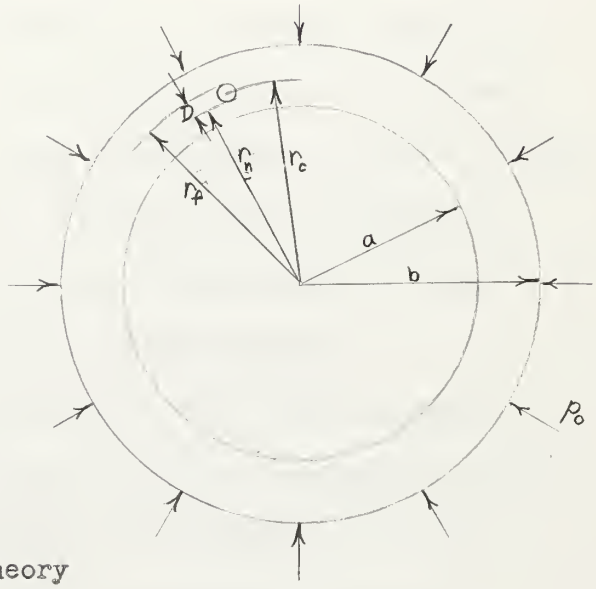

DIMENSIONS READINGS

a = 3.00" p_o = 100 PSI

b = 4.00"

t = 0.505"

D = 0.25"

r_n = 3.37" n_n = 4.8 orders

r_f = 3.62" n_f = 4.3 orders

r_c = 3.495"

From (18) for thick wall cylinder theory

$$\sigma_{tangential} = \sigma_t = -\, p_o b^2/(b^2-a^2)\ [1+a^2/r^2]$$

$$\sigma_{radial} = \sigma_r = -\, p_o b^2/(b^2-a^2)\ [1-a^2/r^2]$$

at r = 3.00" (location of maximum tangential stress for the model if no holes were present)

$$\sigma_{t_{3.00"}} = \frac{-(100)(16)}{16-9}\left[1+\frac{9}{9}\right] = 457.14 \text{ PSI}$$

$$\sigma_{r_{3.00"}} = \frac{-(100)(16)}{16-9}\left[1-\frac{9}{9}\right] = 0.0 \text{ (free boundary in radial direction)}$$

The fringe constant "f" of this material was 83.5lbs/(in)(order).

$$\sigma_t = fn/t = (83.5)(n)/0.505 = 165.3n$$

at r = 3.37" σ_t = (165.3)(4.8) = 794 PSI (larger governs)

at r = 3.62" σ_t = (165.3)(4.3) = 711 PSI

SCF = σ_t(largest for hole)/σ_t(largest for model without holes)

$$SCF_{3.495"} = 794/457 = 1.74$$

D. SUPPLEMENTARY DISCUSSION

PHOTOELASTIC DESCRIPTION

The photoelastic method of analization is an accurate means of determining the stress distribution throughout a model. It is based on the theory of double refraction being proportional to maximum stress at a point in a model. A polariscope, loading frame, and method of fabricating stress free models are the only items needed to obtain visually the stress distribution through photoelasticity.

A plane polariscope consists of a light source with a polarizer and analyzer. The light source for this particular photoelastic study was white light from an incandescent lamp. This lamp emits radient energy that is omni-directional with all wave lengths present. The polarizer filters the light and only allows the vibrations of light in one plane to pass through its privileged axis.

As the polarized beam of white light passes from the polarizer into the transparent plastic model of thickness "t" the light vector splits. This split is dependent upon the index of refraction of the photoelastic material. It is directly proportional to the stresses in the model within the linear range of the stress-strain curve of the model material. Let 1 and 2 represent the directions of principal stresses at a particular point in the model, σ_1 and σ_2 represent the stresses in these directions, and V_1 and V_2 represent the speed of the light in these directions. The time interval for the light to pass through the model will be $\frac{t}{V}$. The phase difference between the two beams of light waves emerging from the

model is

$$\delta = C\left(\frac{t}{V_1} - \frac{t}{V_2}\right) = t\,(n_1 - n_2)$$

where: δ = relative retardation measured in inches between the two phases

C = proportionality constant depending on velocity of light

$n = \frac{C}{V}$ = refractive index of the material.

Brewster (6) established the law that the relative change in index of refraction of photoelastic materials is proportional to the differences of principal stresses or in equation form

$$(n_1 - n_2) = K(\sigma_1 - \sigma_2)$$

where K is a dimensionless constant of the material, termed "strain-optical coefficient". From Brewster's Law and the previous equation comes the basis of photoelasticity that

$$\delta = tK(\sigma_1 - \sigma_2)$$

Determination of the phase difference is therefore a measure of difference between the principal stresses.

These split light vectors after leaving the model arrive at the analyzer. The analyzer passes without alteration any light which is parallel to its privileged axis in a manner similar to that of the polarizer. This single plane of light will be visible to the human eye if in the range of human perception from 4000 to 8000 Angstrom* units.

As the analyzer is rotated in its plane through 90°, either clockwise or counterclockwise, the magnitude of the light that was undisturbed when parallel to the analyzer's privileged axis diminishes till at the

* 1 Angstrom = 10^{-8} cm.

90° position complete extinction of the light occurs. The amplitude of vibrating light "A" that is observed is therefore a function of the angle between the original plane of vibration and the principal plane of stress designated "α" and also the phase difference "δ".

With monochromatic light (one wave length present) dark spots are observed at points where

$$A \sin 2\alpha \sin \delta = 0$$

These dark spots are linked together in a fringe to form loci of constant difference ($\sigma_1 - \sigma_2$) between the principal stresses and are called isocramatics (cases where $\frac{\delta}{2} = 0^{\circ}, 180^{\circ}, \ldots, n$). Also present are dark lines representing the loci of constant stress directions called isoclinics (cases where $\alpha = 0^{\circ}$ or 90°).

For this particular study the isoclinics are redundant and therefore eliminated by converting the plane polariscope described to a circular polariscope. This is accomplished by the insertion of quarter-wave plates on either side of the model. With the circular polariscope one may determine differences between principal stresses and the value of the principal stress along free boundaries where σ_2 goes to zero.

With white light, which is used for this investigation, the dark areas mentioned above in conjunction with monochromatic light are not obtained except where $\delta = 0$, caused by $\sigma_1 - \sigma_2 = 0$. If at a point in the model there is complete extinction of a particular wave length the complementary color will appear. For example, if the wave length of red is extinct, the complementary color green will appear. The most accurate visual observations are made when, at points under investigation,

the yellow of the spectrum is just a tint. This causes a transition to appear between two contrasting bands of green and red. This tint of yellow is accomplished by rotation of the analyzer lens.

The tint of the yellow and the color spectrum visual display are the main advantages of using white light versus monochromatic light. It is easier to determine the tint of yellow than the center of the black fringe as seen with monochromatic light. The color spectrum with its sequence in the direction of increasing stress (yellow-red-green-yellow-red-green,etc.) makes it a great deal easier to identify different fringe orders (No.1, No.2, No.3, etc.). By counting fringe orders and fractions thereof, it is possible to measure directly the magnitude of stresses in the model.

Prior to measuring magnitudes of stresses the fringe constant must be correlated with the material. The equation of the fringe constant is

$$f = \frac{t(\sigma_1 - \sigma_2)}{n} \qquad \text{measured in} \quad \frac{\text{lb.}}{\text{in. x order}}$$

where: n = order of interference.

This fringe constant is the strain necessary to produce one fringe. The lower the fringe constant the more sensitive the model material.

Measurement of the fringe constant of the material is accomplished by making a test sample out of the sheet of material to be used for the model. This test sample is then accurately measured in tension and observed visually to determine fringe order versus load applied. With this data a calibration curve (See Appendix E, Figure V) can be drawn which is used in conjunction with actual testing. The tension test is used although the model will be in compression because the tension method eliminates any buckling effect and is more accurate.

E. ORIGINAL DATA

FIGURE V.

CALIBRATION OF PHOTOELASTIC MATERIAL THROUGH TENSION TEST

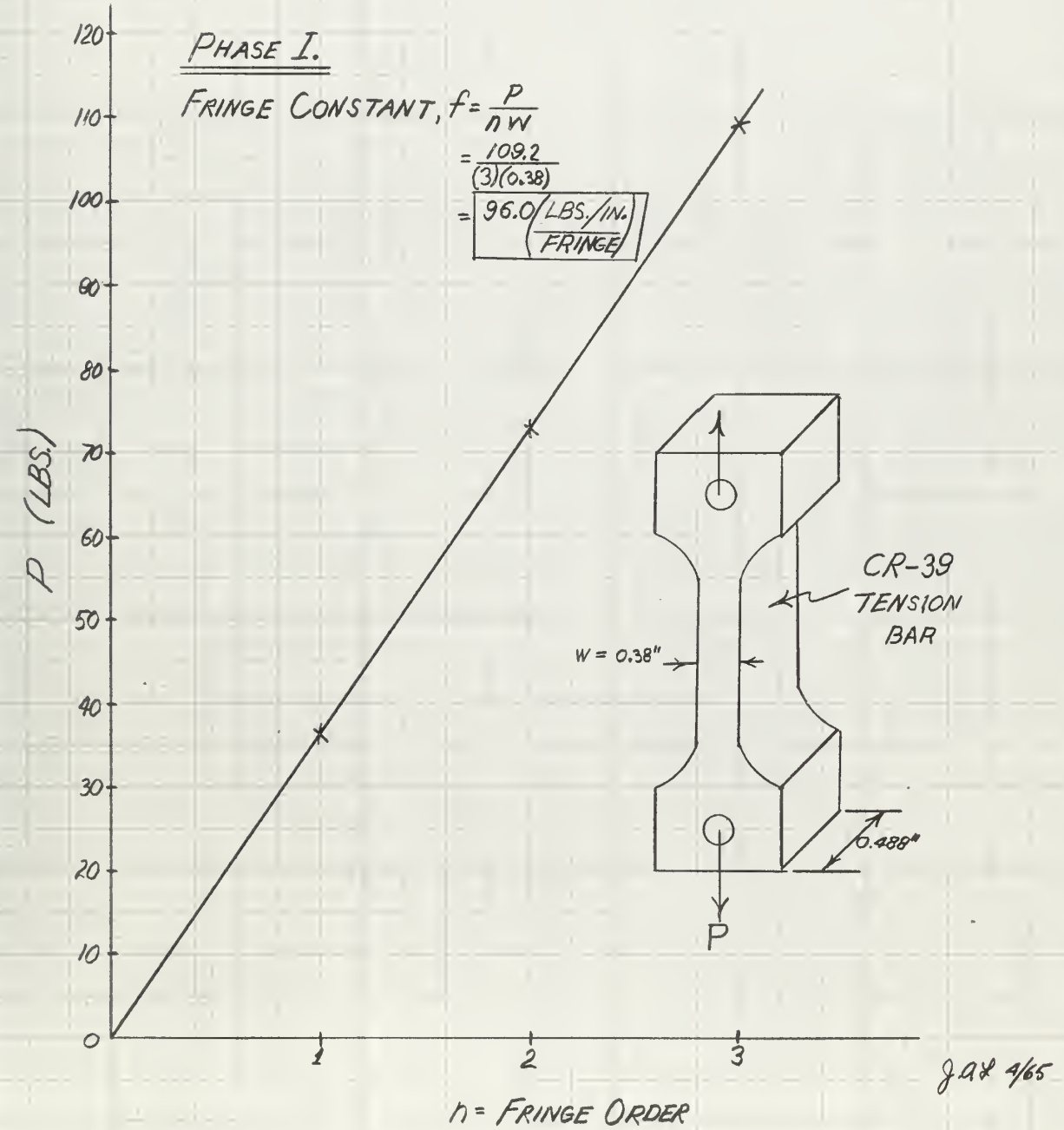

FIGURE VI.

"K" VERSUS SCF_A FOR 6" x 6" MODELS

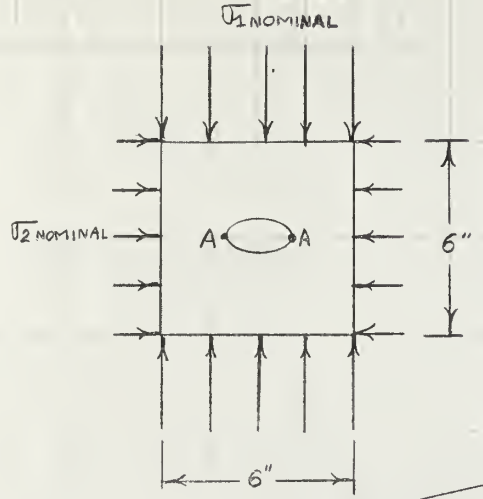

$$K = \frac{\sigma_1 \text{ NOMINAL}}{\sigma_2 \text{ NOMINAL}}$$

JAZ 9/65

FIGURE VII.

"K" VERSUS SCF_A FOR 6" x 5" MODELS

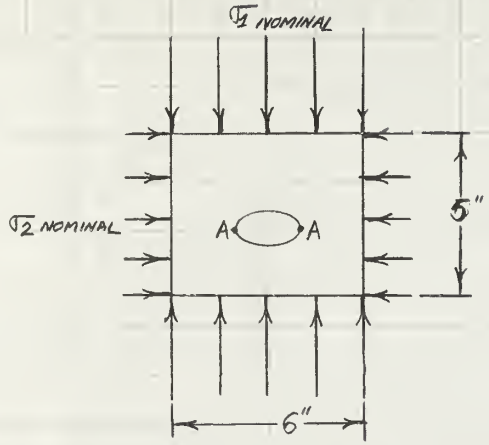

$$K = \frac{\sigma_1 \text{ NOMINAL}}{\sigma_2 \text{ NOMINAL}}$$

ELLIPSE (a/b = 1.84)
ELLIPSE (a/b = 1.42)
ELLIPSE (a/b = 1.11)
CIRCLE (a/b = 1.00)

$SCF_A \rightarrow$

4.0
3.5
3.0
2.5
2.0

1.0 2.0 3.0 4.0 $K \rightarrow$ 5.0 6.0 7.0 8.0

JOL 9/65

FIGURE VIII.

"K" VERSUS SCF_A FOR 6" × 4½" MODELS

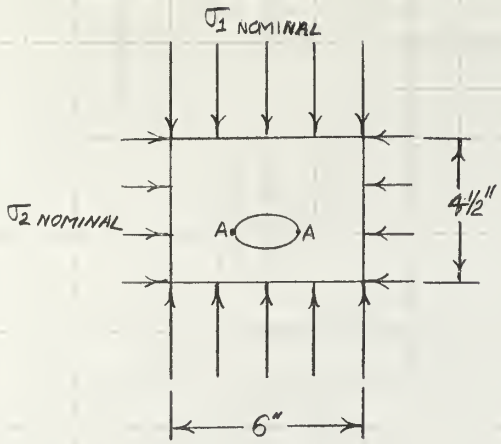

$$K = \frac{\sigma_1 \text{ NOMINAL}}{\sigma_2 \text{ NOMINAL}}$$

ELLIPSE (a/b = 1.84)
ELLIPSE (a/b = 1.42)
ELLIPSE (a/b = 1.11)
CIRCLE (a/b = 1.00)

SCF_A →

4.0
3.5
3.0
2.5
2.0

1.0 2.0 3.0 4.0 K → 5.0 6.0 7.0 8.0

JAS 4/65

FIGURE IX.

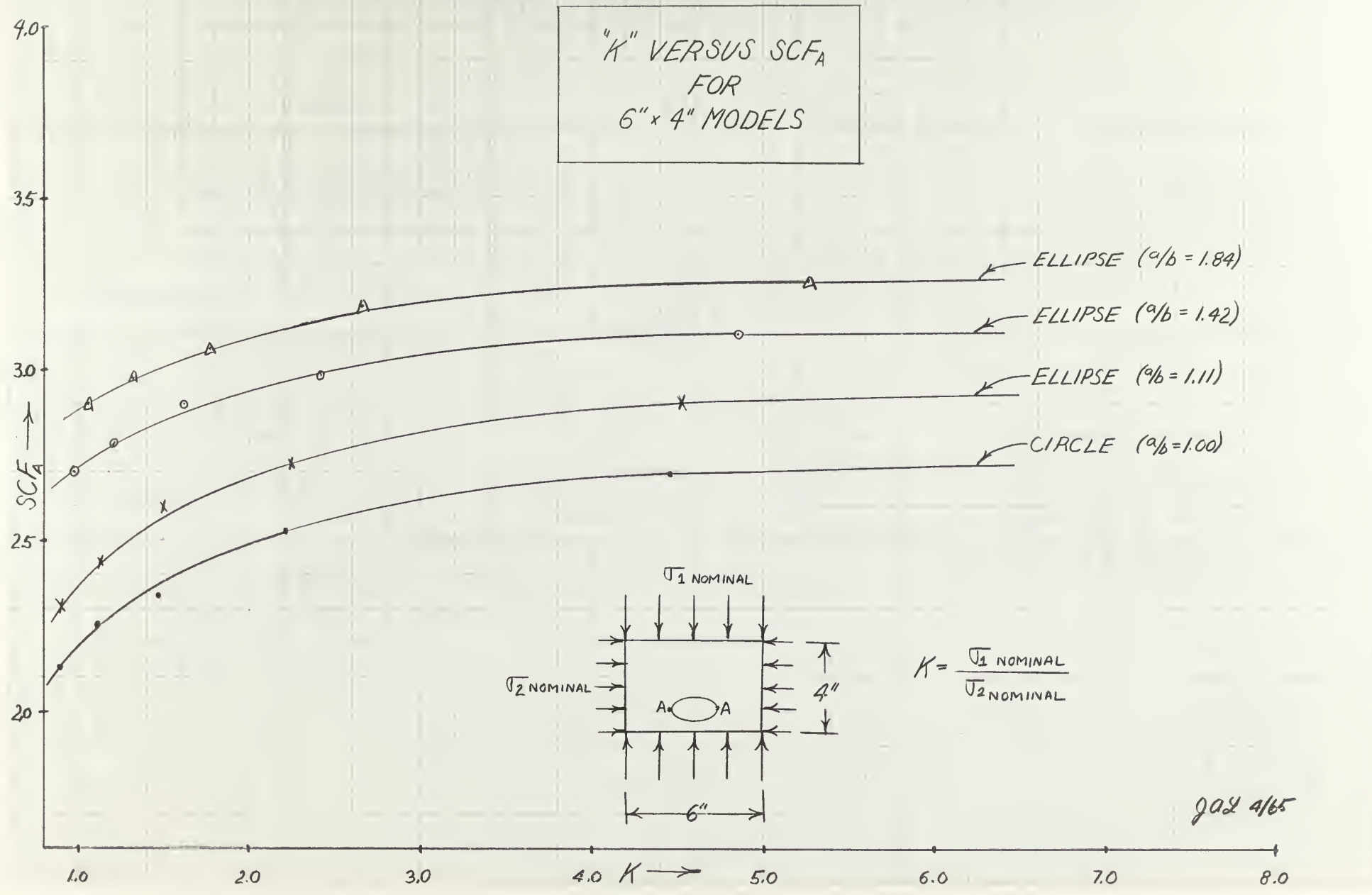
"K" VERSUS SCF_A
FOR
6" x 4" MODELS
4.0
3.5
3.0
2.5
2.0
SCF_A
ELLIPSE (a/b = 1.84)
ELLIPSE (a/b = 1.42)
ELLIPSE (a/b = 1.11)
CIRCLE (a/b = 1.00)
σ_1 NOMINAL
σ_2 NOMINAL
A
A
4"
6"
$K = \frac{\sigma_1 \text{ NOMINAL}}{\sigma_2 \text{ NOMINAL}}$
JAL 4/65
1.0
2.0
3.0
4.0
K
5.0
6.0
7.0
8.0

FIGURE X.

"K" VERSUS SCF_A FOR CIRCLE MODEL

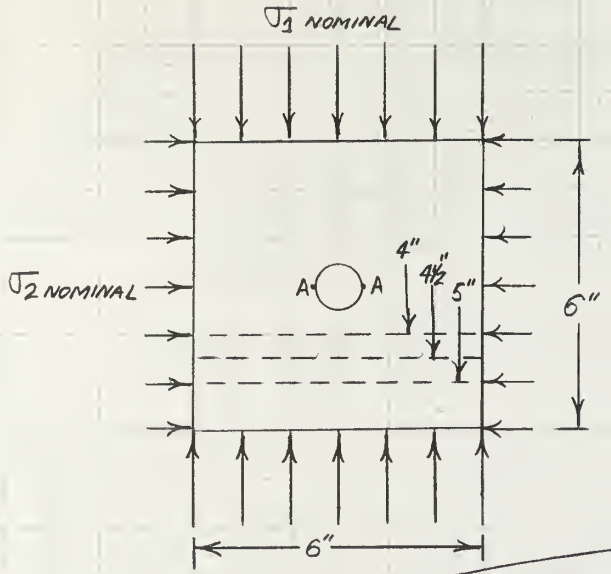

$$K = \frac{\sigma_1 \text{ NOMINAL}}{\sigma_2 \text{ NOMINAL}}$$

JAZ 4/65

FIGURE XI.

"K" VERSUS SCF_A FOR ELLIPSE - a/b = 1.11

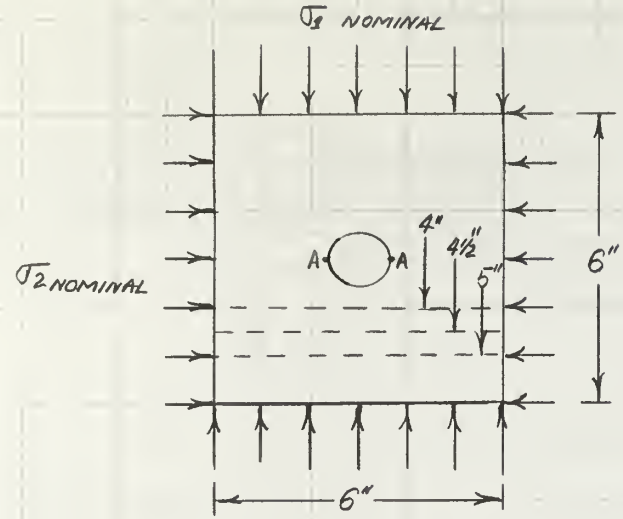

$$K = \frac{\sigma_1 \text{ NOMINAL}}{\sigma_2 \text{ NOMINAL}}$$

ELLIPSE - a/b = 1.11 (6" x 4")

ELLIPSE - a/b = 1.11 (6" x 4½")

ELLIPSE - a/b = 1.11 (6" x 5")

ELLIPSE - a/b = 1.11 (6" x 6")

SCF_A →

4.0
3.5
3.0
2.5
2.0

1.0 2.0 3.0 4.0 K → 5.0 6.0 7.0 8.0

JAZ 4/65

41

FIGURE XII.

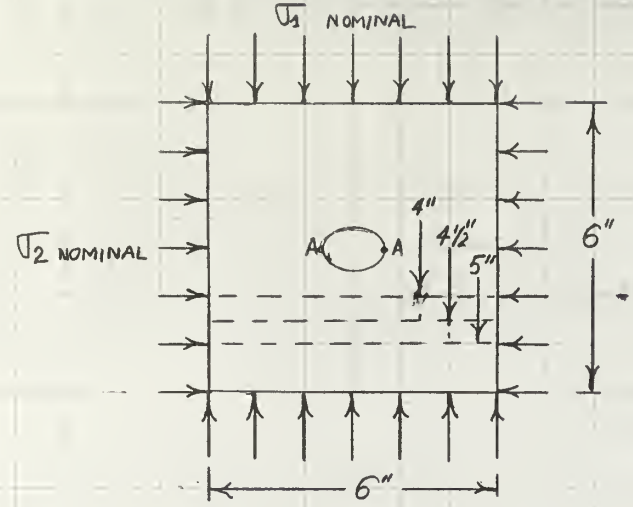

"K" VERSUS SCF_A FOR ELLIPSE - a/b = 1.42

$$K = \frac{\sigma_1 \text{ NOMINAL}}{\sigma_2 \text{ NOMINAL}}$$

ELLIPSE - a/b = 1.42 (6" x 4")

ELLIPSE - a/b = 1.42 (6" x 4½")

ELLIPSE - a/b = 1.42 (6" x 5")

ELLIPSE - a/b = 1.42 (6" x 6")

SCF_A →

K →

4.0
3.5
3.0
2.5
2.0

1.0
2.0
3.0
4.0
5.0
6.0
7.0
8.0

JAZ 4/65

FIGURE XIII.

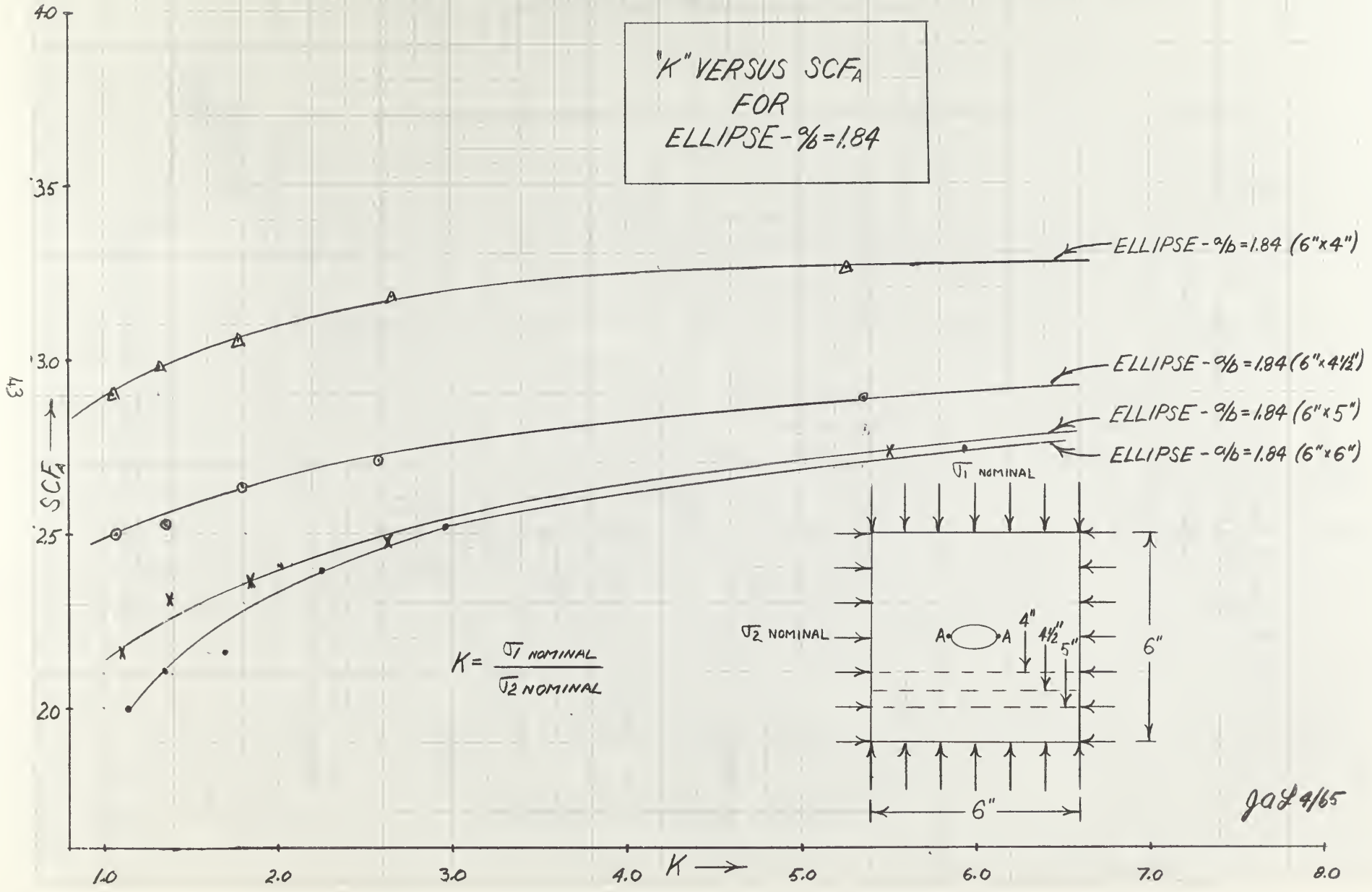
"K" VERSUS SCF_A
FOR
ELLIPSE - a/b = 1.84
ELLIPSE - a/b = 1.84 (6" x 4")
ELLIPSE - a/b = 1.84 (6" x 4½")
ELLIPSE - a/b = 1.84 (6" x 5")
ELLIPSE - a/b = 1.84 (6" x 6")
SCF_A
K
$K = \frac{\sigma_1 \text{ NOMINAL}}{\sigma_2 \text{ NOMINAL}}$
σ_1 NOMINAL
σ_2 NOMINAL
A
A
4"
4½"
5"
6"
6"
4.0
3.5
3.0
2.5
2.0
1.0
2.0
3.0
4.0
5.0
6.0
7.0
8.0
JAL 4/65

FIGURE XIV.

NOMOGRAPH TO DIRECTLY RELATE FRINGE ORDER AT ANY RADIUS "R" TO HYDROSTATIC PRESSURE

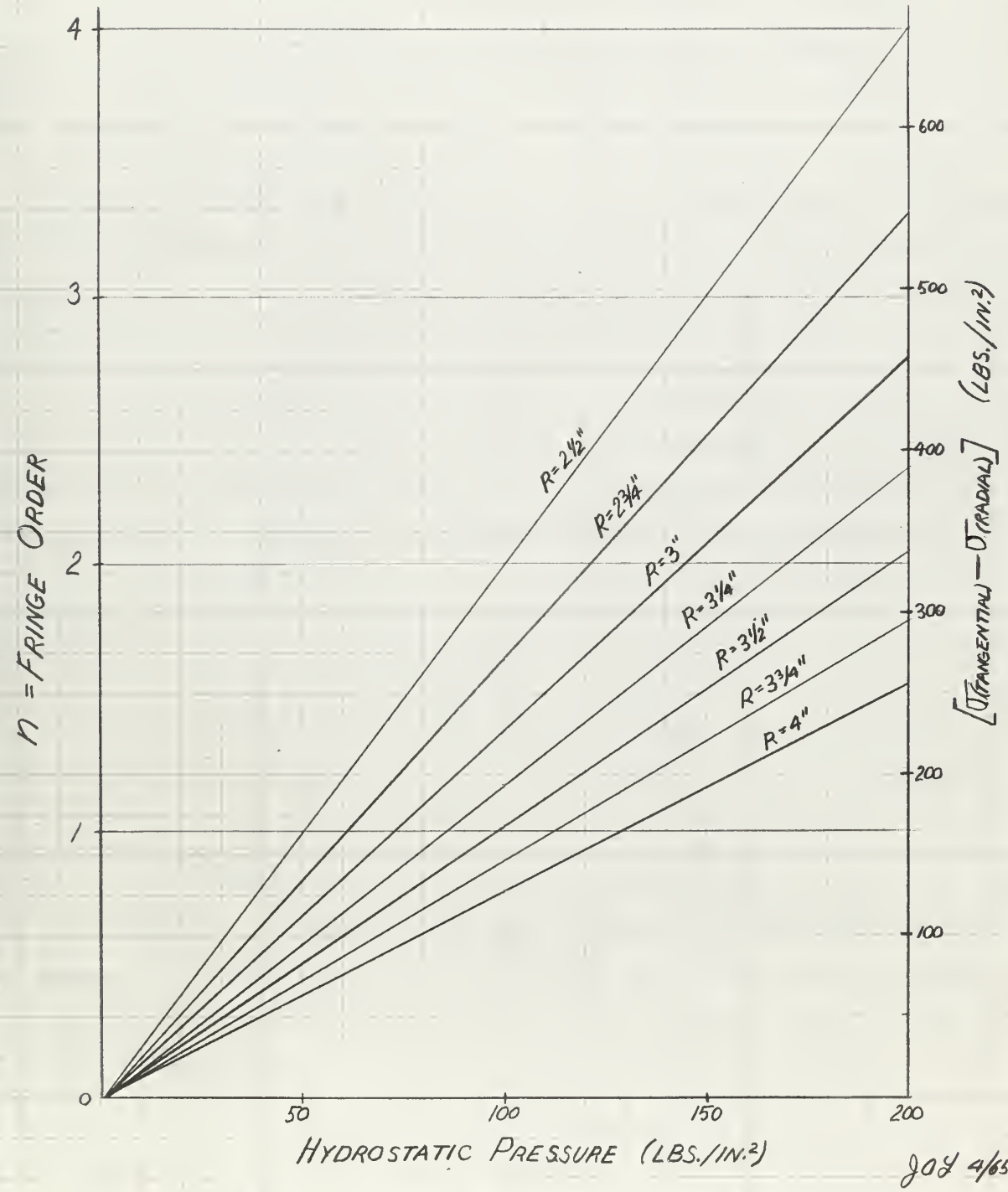

JOY 4/65

FIGURE XV.

STRESS PATTERNS FOR 1" WEB WITH 1½"x¼" FLANGE

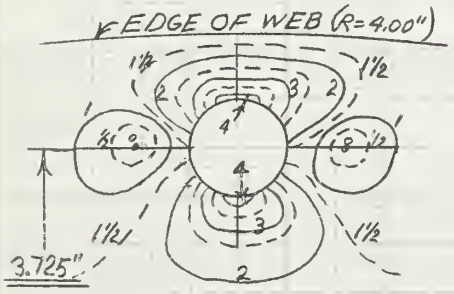

STRESS GRADIENTS FOR 1" WEB WITH 1½"x ¼" FLANGE

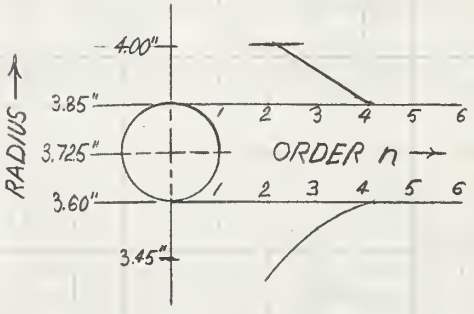

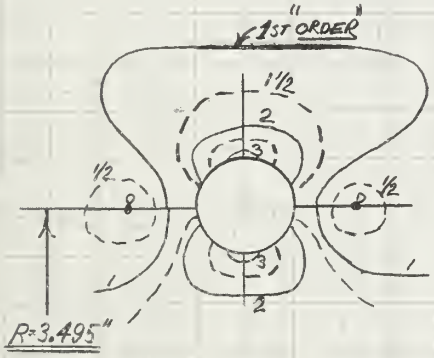

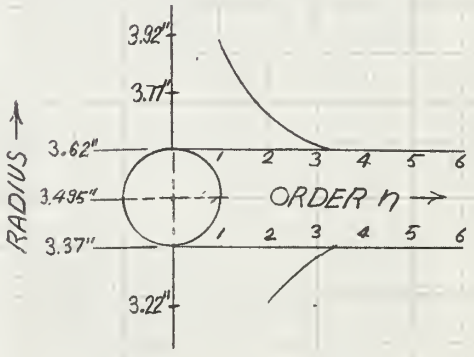

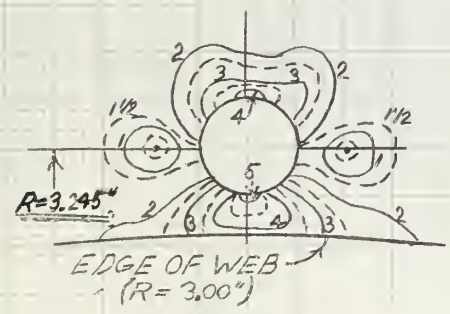

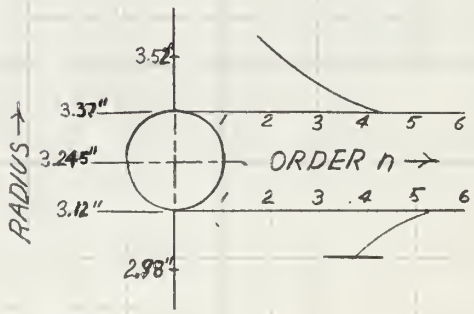

TABLE III.
FRINGE ORDERS VERSUS RADIUS
(PHASE II.)

3.725"RADIUS TO CENTER OF HOLE		3.625"RADIUS TO CENTER OF HOLE		3.495"RADIUS TO CENTER OF HOLE		3.375"RADIUS TO CENTER OF HOLE		3.245"RADIUS TO CENTER OF HOLE	
ORDER	RADIUS	ORDER	RADIUS	ORDER	RADIUS	ORDER	RADIUS	ORDER	RADIUS
1½"WEB WITHOUT FLANGE									
3.0	3.52	2.0	3.38	2.5	3.29	3.0	3.17	3.0	3.01
3.5	3.55	2.5	3.40	3.0	3.32	3.5	3.19	3.5	3.05
4.0	3.56	3.0	3.44	3.5	3.34	4.0	3.21	4.0	3.07
4.5	3.59	3.5	3.46	4.0	3.35	4.5	3.24	5.2	3.12
5.0	3.60	4.0	3.48	4.6	3.37	4.8	3.25	HOLE	
HOLE		4.5	3.50	HOLE		HOLE		4.7	3.37
4.8	3.85	HOLE		3.9	3.62	3.8	3.50	4.0	3.39
4.5	3.86	4.1	3.75	3.5	3.64	3.5	3.51	3.5	3.41
4.0	3.88	3.5	3.77	3.0	3.67	3.0	3.53	3.0	3.42
3.5	3.90	3.0	3.79	2.5	3.69	2.5	3.56	2.5	3.51
3.0	3.93	2.5	3.81	2.0	3.74	2.0	3.62	2.0	3.53
2.5	3.95	2.0	3.87	1.5	3.79				
2.0	3.98								
1½"WEB WITH FLANGE									
1.5	3.45	1.0	3.26	1.5	3.26	2.0	3.15	2.0	3.02
2.0	3.52	1.5	3.39	2.0	3.30	2.5	3.18	2.5	3.05
2.5	3.54	2.0	3.44	2.5	3.32	3.0	3.21	3.0	3.07
3.0	3.57	2.5	3.45	3.0	3.36	3.6	3.25	4.1	3.12
3.5	3.59	3.0	3.48	3.2	3.37	HOLE		HOLE	
3.8	3.60	3.5	3.50	HOLE		3.5	3.50	3.8	3.37
HOLE		HOLE		3.3	3.62	2.5	3.54	3.0	3.40
3.8	3.85	3.4	3.75	2.0	3.67	2.0	3.57	2.5	3.44
3.5	3.87	3.0	3.77	1.5	3.70	1.5	3.62	2.0	3.45
3.0	3.90	2.5	3.79	1.0	3.75			1.5	3.51
2.5	3.91	2.0	3.82	0.5	3.88			1.0	3.67
2.0	3.96	1.5	3.86						
1.5	3.98	1.0	3.93						

TABLE III, Continued

3.725"RADIUS TO CENTER OF HOLE		3.625"RADIUS TO CENTER OF HOLE		3.495"RADIUS TO CENTER OF HOLE		3.375"RADIUS TO CENTER OF HOLE		3.245"RADIUS TO CENTER OF HOLE	
ORDER	RADIUS	ORDER	RADIUS	ORDER	RADIUS	ORDER	RADIUS	ORDER	RADIUS
1" WEB WITHOUT FLANGE									
2.5	3.50	2.0	3.31	3.0	3.27	3.5	3.09	6.0	3.06
3.0	3.53	2.5	3.38	3.5	3.30	4.0	3.15	7.4	3.12
3.5	3.54	3.0	3.41	4.0	3.32	4.5	3.19	HOLE	
4.0	3.56	3.5	3.44	4.5	3.36	5.0	3.21	5.7	3.37
4.5	3.58	4.0	3.46	4.8	3.37	6.0	3.25	5.5	3.38
5.6	3.60	4.9	3.50	HOLE		HOLE		5.0	3.41
HOLE		HOLE		4.3	3.62	4.8	3.50	4.5	3.45
4.7	3.85	4.5	3.75	4.0	3.65	4.5	3.51	4.0	3.48
4.5	3.86	4.0	3.77	3.5	3.69	4.0	3.52	3.5	3.50
4.0	3.89	3.5	3.79	3.0	3.75	3.5	3.56	3.0	3.52
3.5	3.91	3.0	3.84	2.5	3.78	3.0	3.61	2.5	3.64
3.0	3.96	2.5	3.91			2.5	3.69		
2.5	3.97								
2.0	4.00								
1" WEB WITH FLANGE									
2.0	3.42	2.0	3.38	2.0	3.25	2.5	3.10	4.0	3.03
2.5	3.50	2.5	3.42	2.5	3.29	3.0	3.17	4.5	3.07
3.0	3.54	3.0	3.45	3.0	3.34	3.5	3.19	5.0	3.10
3.5	3.56	3.5	3.49	3.3	3.37	4.3	3.25	5.2	3.12
4.0	3.59	3.7	3.50	HOLE		HOLE		HOLE	
4.2	3.60	HOLE		3.2	3.62	3.5	3.50	4.3	3.37
HOLE		3.6	3.75	3.0	3.63	3.0	3.52	4.0	3.38
4.1	3.85	3.0	3.80	2.5	3.68	2.5	3.56	3.5	3.40
4.0	3.86	2.5	3.82	2.0	3.73	2.0	3.62	3.0	3.42
3.5	3.90	2.0	3.87	1.5	3.81			2.5	3.48
3.0	3.94	1.5	3.92	1.0	3.94			2.0	3.52
2.5	3.96								
2.0	3.98								
1.5	4.00								

F. LITERATURE CITATION

1. Berge, N. K. and Sweeney, J. A., Photoelastic Analysis of Reinforced Circular Holes in Plates Under Compression, Massachusetts Institute of Technology Thesis, May, 1960.

2. Coker, E. G. and Filon, L. N., A Treatise on Photo-Elasticity, Cambridge University Press, 1931.

3. Crites, N. A. and Hunter A. R., "Experimental Stress Analysis by Photoelastic Techniques", Product Engineering, September, 1962.

4. Durelli, A. J. and Murray, W. M., "Stress Distribution Around an Elliptical Discontinuity in Any Two-Dimensional, Uniform and Axial, System of Combined Stress", Proceedings of the Society for Experimental Stress Analysis, Vol. I, No. 1, 1943.

5. Eshbach, O. W., Handbook of Engineering Fundamentals, John Wiley and Sons, New York, 1948.

6. Frocht, M. M., Photo-Elasticity, Vol. I, John Wiley and Sons, New York, 1948.

7. Frocht, M.M., Photo-Elasticity, Vol. II, John Wiley and Sons, New York, 1948.

8. Griffel, W., "Stress Concentration Factors for Plates with Holes", Product Engineering, September, 1963.

9. Griffel, W., "More Concentration Factors for Stresses Around Holes", Product Engineering, November, 1963.

10. Heller, S. R. Jr., Reinforced Circular Holes in Bending with Shear, Massachusetts Institute of Technology Thesis, June, 1953.

11. Hetenyi, M., Handbook of Experimental Stress Analysis, John Wiley and Sons, New York, 1961.

12. Lipson, C. and Juvinall, R. C., Handbook of Stress and Strength Design and Material Applications, MacMacmillan Company, New York, 1963.

13. Mathews, E. S., Photoelastic Examination of Stresses in a Thick Hollow Cylinder, Massachusetts Institute of Technology Thesis, June, 1940.

14. Murray, W. M., and Stein, P. K., Strain Gage Techniques, Society for Experimental Stress Analysis, 1961.

15. Peterson, R. E., Stress Concentration Design Factors, John Wiley and Sons, New York, 1953.

16. Savin, G. N., Stress Concentrations Around Holes, Pergamon Press, 1962.

17. Timoshenko, S., Strength of Material, D. Van Nostrand Company, New York, 1941.

18. Timoshenko, S., Theory of Elasticity, McGraw-Hill, New York, 1951.

19. Design Data Sheet 1100-1, Department of the Navy, Bureau of Ships, 19 March, 1950.

20. "Experimental Stress Analysis", Product Engineering, April, 1948.

21. "Introduction to Stress Analysis by Photo-Elastic Coating Technique", Technical Data Bulletin TDG-1, Photolastic Incorporated, October, 1963.

22. Stress Analysis by the Photoelastic Method, Chapman Laboratories, 1963.